catalysts

MDPI

Article

Heterometallic $Co^{III}Zn^{II}$ Schiff Base Catalyst for Mild Hydroxylation of C(sp^3)–H Bonds of Unactivated Alkanes: Evidence for Dual Mechanism Controlled by the Promoter

Oksana V. Nesterova [1,*], Katerina V. Kasyanova [2], Elena A. Buvaylo [2], Olga Yu. Vassilyeva [2,*], Brian W. Skelton [3], Dmytro S. Nesterov [1] and Armando J.L. Pombeiro [1,*]

1 Centro de Química Estrutural, Instituto Superior Técnico, Universidade de Lisboa, Av. Rovisco Pais, 1049-001 Lisboa, Portugal; dmytro.nesterov@tecnico.ulisboa.pt
2 Department of Chemistry, Taras Shevchenko National University of Kyiv, 64/13 Volodymyrska str., Kyiv 01601, Ukraine; kasyanova.kv@gmail.com (K.V.K.); vinograd@univ.kiev.ua (E.A.B.)
3 School of Molecular Sciences, M310, University of Western Australia, Perth, WA 6009, Australia; brian.skelton@uwa.edu.au
* Correspondence: oksana.nesterova@tecnico.ulisboa.pt (O.V.N.); vassilyeva@univ.kiev.ua (O.Y.V.); pombeiro@tecnico.ulisboa.pt (A.J.L.P.)

Received: 29 January 2019; Accepted: 13 February 2019; Published: 26 February 2019

Abstract: The novel Schiff base complex $[Co^{III}Zn^{II}L_3Cl_2]\cdot CH_3OH$ (**1**) was synthesized by interaction of zinc powder, cobalt(II) chloride and methanol solution of the pre-formed HL in air (HL is the product of condensation of *o*-vanillin and methylamine) and characterized by IR, UV-Vis and NMR spectroscopy, ESI-MS and single crystal X-ray diffraction analysis. In the heterometallic core of **1** the two metal centers are bridged by deprotonated phenoxy groups of the L^- ligands with the cobalt-zinc separation of 3.123 Å. Catalytic investigations demonstrated a pronounced activity of **1** towards mild alkane oxidation with *m*-chloroperbenzoic acid (*m*-CPBA) as an oxidant and *cis*-1,2-dimethylcyclohexane (*cis*-1,2-DMCH) as the model substrate. The influence of the nature of different promoting agents of various acidities (from HOTf to pyridine) on the catalytic process was studied in detail and a pronounced activity of **1** in the presence of nitric acid promoter was found, also showing a high retention of stereoconfiguration of the substrate (>99% for *cis*-1,2-DMCH). The best achieved yield of tertiary *cis*-alcohol based on the oxidant was 61%, with a turnover number (TON) of 198 for nitric acid as promoter. The ^{18}O-incorporations into the alcohols when the reactions were performed under $^{18}O_2$ atmosphere using acetic and nitric acid promoters, suggest that the *cis*-1,2-DMCH hydroxylation proceeds by two distinct pathways, a non-stereoselective and a stereoselective one (with and without involvement of a long-lived free carbon radical, respectively). The former dominates in the case of acetic acid promoter and the latter is realized in the case of HNO_3 promoter.

Keywords: stereoselective C-H oxidation; metal complex catalysis; ^{18}O isotopic labelling

1. Introduction

Selective transformation of inactive aliphatic C−H bonds into suitable functional groups is a principal goal of modern chemistry [1–8]. Among the already developed approaches towards the C–H activation, those capable of selective insertion of oxygen into a particular sp^3 carbon–hydrogen bond are less numerous and often are limited to specific positions (e.g. allylic sites) or require laborious synthesis of catalysts [9,10]. Additional challenges are encountered in stereoselective C−H oxidations.

It is known that metalloenzymes, such as cytochrome P450 or methane monooxygenase (MMO), can functionalize C–H bonds of a range of substrates, including alkanes, under very mild conditions and using dioxygen or peroxides as terminal oxidants [11–14]. These observations inspired chemists to synthesize families of complexes, primarily of copper, iron and manganese, which could mimic the reaction mechanisms of enzymatic oxidations [15]. Nowadays these families are represented mainly by porphyrin complexes and a few classes of non-heme systems, mostly based on N-donor macrocyclic or polypyridyl ligands [13,15–17].

Catalytic activity of cobalt complexes in the oxidative functionalization of sp^3 C–H bonds is much less explored than that of iron or manganese compounds, although there is clear evidence that cobalt species may serve as highly efficient and selective catalysts [18–25]. We recently reported a cobalt complex with a simple N,O-donor isoindole ligand, which revealed a high stereoselectivity in the course of oxidation of sp^3 C–H bonds using *m*-chloroperoxybenzoic acid (*m*-CPBA) oxidant [26]. Being interested in better understanding of the mechanism of the retention of stereoconfiguration and following our long-term interest in polynuclear coordination compounds [2,27], we have prepared a novel cobalt complex bearing a similar N,O-donor ligand, but decorated with a second redox inactive metal, $[Co^{III}Zn^{II}L_3Cl_2]\cdot CH_3OH$ (**1**) (HL = 2-methoxy-6-[(methylimino)methyl]phenol, Scheme 1). It was recently shown that non-redox metals, such as zinc, cadmium, bismuth *etc*., may influence the redox reaction pathway or even serve as the main catalysts [28–32]. Thus, we were motivated to study the catalytic properties of the heterometallic Co^{III}/Zn^{II} complex **1** in the oxidation of alkanes using *m*-CPBA as terminal oxidant.

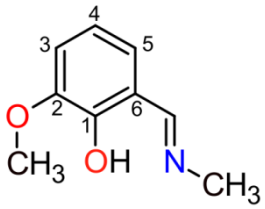

Scheme 1. Structural formula for 2-methoxy-6-[(methylimino)methyl]phenol, HL.

It is known that common C–H hydroxylation pathways (such as radical rebound, concerted, metal-mediated or free radical one) show drastically different ^{18}O-incorporations into the final products, alcohols, from various sources, first of all $^{18}O_2$, $H_2{}^{18}O$ and ^{18}O-labelled peroxides [33–36]. For example, the use of $^{18}O_2$, in combination with bond-, regio- and stereoselectivity data, provides evidence about the participation (or non-participation) of a long-lived free carbon radical in the catalytic mechanism [2,36–41]. However, this important area still remains underdeveloped.

The heterometallic **1** was prepared using a one-pot reaction of zinc powder with cobalt(II) chloride in methanol in the presence of HL formed *in situ* in open air. Details and applications of the used synthetic approach were given earlier by some of us [27]. Herein, we report on the synthesis, crystal structure and spectroscopic characterization of complex **1**, as well as its catalytic activity towards stereoselective alkane oxidation with *m*-CPBA in the presence of various promoting agents under mild conditions. To get insights into the type of reaction mechanism, we performed a combined selectivity/$^{18}O_2$ study.

2. Results and Discussion

2.1. Synthesis and crystal structure

The Schiff base HL was synthesized *in situ* by condensation of *o*-vanillin and $CH_3NH_2\cdot HCl$ in methanol in the presence of dimethylaminoethanol. The one-pot reaction of zinc powder, cobalt chloride hexahydrate and the pre-formed HL in methanol using the $Zn^0 : CoCl_2 : HL = 1 : 1 : 3$ mole ratio in open air resulted in the formation of a brown-colored solution. The zerovalent metal was oxidized by atmospheric dioxygen and readily dissolved while the reaction mixture was heated

mildly under magnetic stirring. Dark-red X-ray quality crystals of complex **1** were formed by the following day. The cobalt(II) is easily oxidized to the cobalt(III) species in open air even in the presence of zerovalent zinc. Cobalt(III) oxidation state is effectively stabilized by the deprotonated Schiff base ligand that enables formation of the neutral CoL_3 species with the metal center in a *mer* configuration (see below). The latter acts as a metalloligand to a Zn^{2+} ion, affording the heterometallic complex **1**.

Complex **1** crystallizes in the monoclinic space group $P2_1/n$. It is built of $[CoZnL_3Cl_2]$ neutral molecules with the metal centers bridged by two deprotonated phenoxy groups from the two L^- ligands. Solvent methanol molecules are involved in O–H···O hydrogen bonding. The molecular diagram of **1** with a numbering scheme is given in Figure 1, while selected bond distances and angles are presented in Table S1.

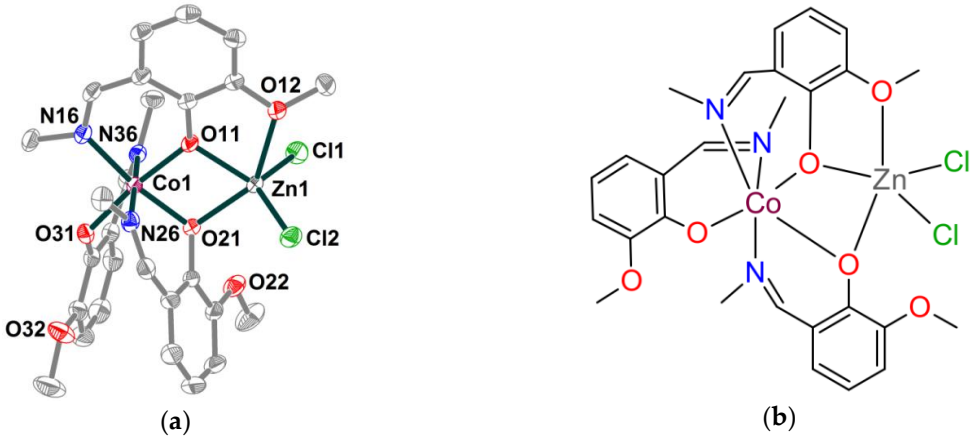

Figure 1. (**a**) Molecular structure of complex **1** with principal atom labelling. Non-H atoms are shown with 70% probability displacement ellipsoids. Selected bond lengths (Å): Co1–O31 1.8788(14), Co1–O11 1.9083(14), Co1–O21 1.9094(14), Co1–N16 1.9436(17), Co1–N26 1.9475(17), Co1–N36 1.9506(17), Zn1–O11 2.0300(14), Zn1–O21 2.1186(14), Zn1–Cl2 2.2183(6), Zn1–Cl1 2.2242(6), Zn1–O12 2.4038(15); (**b**) Chemical scheme of **1**.

The $[CoZnL_3Cl_2]$ molecule that lacks crystallographic symmetry contains two metal atoms in $Co(1)N_3O_3$ and $Zn(1)O_3Cl_2$ distorted octahedral and square-pyramidal geometries, respectively. The oxidation state assignment for the cobalt ion was based on interatomic distances and charge considerations. Three crystallographically non-equivalent Schiff base ligands coordinate the cobalt center through the azomethine nitrogen and phenolate oxygen atoms with Co–O/N bond lengths in the ranges 1.8788(14)–1.9094(14) and 1.9436(17)–1.9506(17), respectively (Figure 1, Table S1). The average Co–O and Co–N bond distances are equal to 1.899 and 1.947 Å, respectively. The *trans* angles at the cobalt atom fall in the range 171.38(7)–175.35(7)°, the *cis* angles vary from 84.82(7) to 94.81(7)° (Table S1). The zinc atom possesses a distorted tetrahedral geometry forming two shorter bonds to the phenolato O atoms of the two L^- ligands, O(11) and O(21) [2.0300(14), 2.1186(14) Å], and two longer bonds to the chlorine atoms [Cl1: 2.2242(6), Cl2: 2.2183(6) Å]. The angles at the metal atom fall in the range 70.79(5)–143.30(5)°. The additional weak Zn–O bond to the methoxy oxygen atom O(12) of 2.4038(15) Å implies that the Zn(1) coordination polyhedron approximates a highly irregular square pyramid with Cl(1) atom in the axial position. The μ-phenoxo-bridged metal centers are separated at 3.123 Å. No significant intermolecular interactions between the dinuclear units are observed in the solid state. The oxygen atom of the solvent methanol molecule, O1, acts as a donor to O31 and O32 atoms of the ligand [O1–H1···O31, 2.790(2), H1···O31, 1.983(13) Å, ∠ = 157(2)°; O1–H1···O32, 3.035(1), H1···O32, 2.434(1) Å, ∠ = 128.17°] forming a five-membered supramolecular synthon (Figure 2, enlarged fragment). Stacked complex molecules form sheets parallel to the *ab* plane with polar methoxy-groups and chloride ligands protruding into the intersheet space and together with solvent molecules keeping the sheets apart (Figure 2). In the solid state, numerous C–H···Cl contacts with the H···Cl distances of well above 2.75 Å are due to van der Waals close packing.

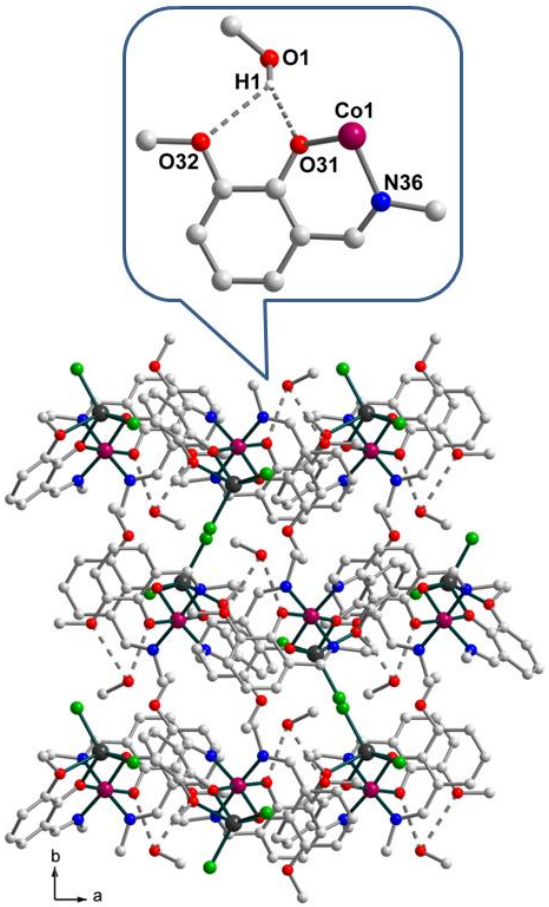

Figure 2. The crystal packing diagram of $[Co^{III}Zn^{II}L_3Cl_2]\cdot CH_3OH$ (**1**) and the enlarged fragment demonstrating H-bonding between the solvent methanol molecule and deprotonated Schiff base ligand. H atoms are not shown. Color scheme: Co, magenta; Zn, dark grey; O, red; N, blue; C, light grey; Cl, green.

2.2. Spectroscopic characterization

The infrared spectrum of complex **1** in the 4000–400 cm^{-1} range contains broad overlapping bands in the region 3600–3400 cm^{-1}, ascribed to the OH group of the methanol solvent molecule (Figure S1). Bands arising above 3000 cm^{-1} are due to aromatic = C–H stretching of the ligand and solvent; their alkyl C–H stretching vibration are seen below 3000 cm^{-1}. The characteristic ν(C=N) peak of L^- is detected at 1630 cm^{-1} (1634 cm^{-1} for free HL, Figure S1). Several sharp bands of medium intensity are observed in the phenyl ring stretching (1600–1400 cm^{-1}) and out-of-plane CH bending regions (800–700 cm^{-1}).

The diamagnetic nature of Co^{III} enabled NMR characterization of **1** in solution. The ^1H NMR spectrum of **1** exhibits the expected set of signals between 8 and 2.5 ppm (Figure S2). The *mer* arrangement of the bidentate deprotonated ligands around the Co(III) atom, which causes the inequivalence of all three coordinated Schiff bases is retained in DMSO solution. The three different ligand environments are clearly distinguished by three different signals in a 1 : 1 : 1 ratio at δ 7.95, 7.79 and 7.46 for the –CH=N– protons, a set of two signals for nine CH_3O protons at δ 3.61, 3.53, in a 1 : 2 ratio and signals of nine aromatic protons due to the three inequivalent rings observed as five doublets, a triplet and a multiplet in the range 6.91–6.22 ppm. The signals of CH_3 protons of the ligand and solvent are partly obscured by a H_2O residual signal.

The ESI-MS spectrum of complex **1** (Figure S3) in CH_3CN (ca. 1×10^{-5} M) shows the strongest peak at 1338 *m/z*, which was associated to dimer of complex **1** $[(Co^{III}L_3)_2Zn_2Cl_3 - H]^+$ (Figure S4). A peak of comparable intensity is observed at 1125 *m/z*, which is assigned to $[(Co^{III}L_3)_2Na - H]^+$

(Figure S5). The molecular ion of **1** was not detected. However, its derivative with eliminated chloride ion, $[\mathbf{1} - Cl^-]^+$ is clearly seen at 650 m/z (Figure 3 and Figure S3), showing the intensity, after correction for isotopic distribution, of 43% relative to the top peak at 1338 *m/z*. Some products of degradation of **1** were also detected as peaks of low intensities, namely $[Co^{III}L_2]^+$ and $[Co^{III}L_3 - e^-]^+$ species at m/z = 387 and 551 *m/z*, respectively (Figure S3). The observed ionization pathways and species formed are typical for ESI-MS spectrometry of coordination compounds [42]. These results suggest that the binuclear core of **1** keeps its integrity even in diluted solutions.

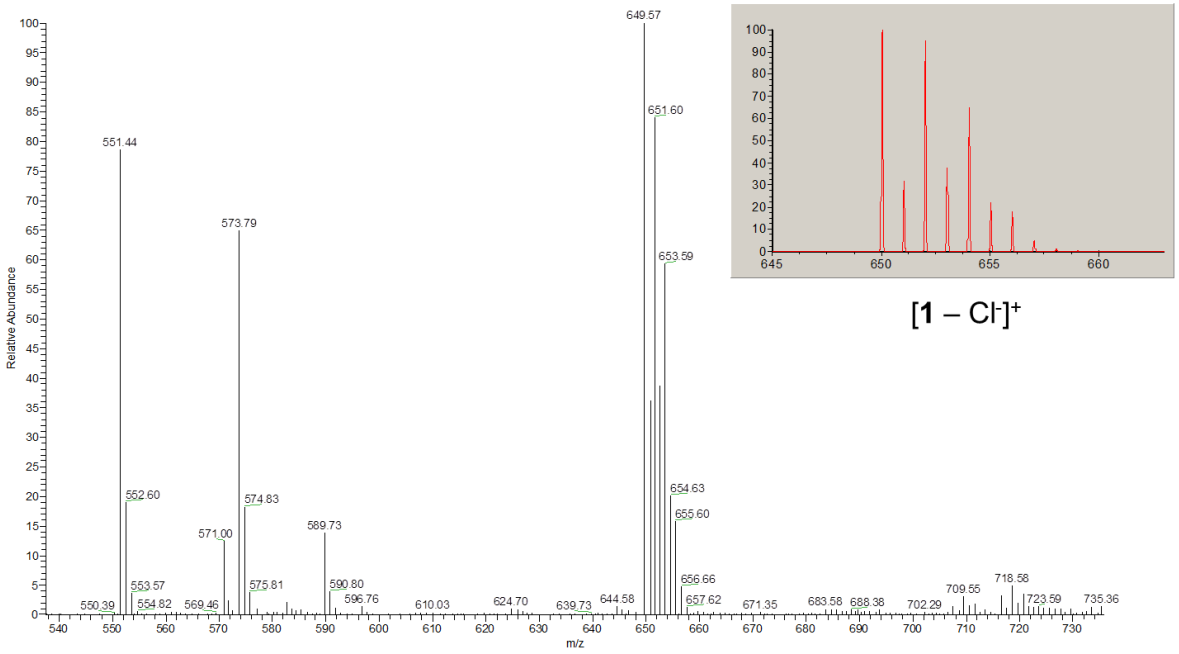

Figure 3. Fragment of the ESI-MS spectrum (Figure S3) in acetonitrile showing the isotopic distribution for the peak at 650 *m/z* attributed to the $[\mathbf{1} - Cl^-]^+$ species. The inset shows calculated distribution for the proposed species.

2.3. Catalytic activity

The catalytic activity of complex **1** was studied in the hydroxylation of sp^3 C–H bonds of unactivated alkanes, under mild conditions. Oxidation of *cis*-1,2-dimethylcyclohexane (*cis*-1,2-DMCH) was chosen as a primary reaction. This substrate is a recognized model that allows simultaneous determination of stereo-, bond- and regio-preferences [2,26,35,43,44]. The reaction of *m*-CPBA, in the presence of nitric acid, with *cis*-1,2-DMCH, using various loadings of **1** (Table 1, Entries 1–3), afforded the tertiary *cis*-alcohol as the main product (Figure S6). The dependence of the initial reaction rate W_0 on [1] was found to be linear, suggesting that no change of the catalyst composition occurs in the studied range of [1] (Figure 4). The extrapolated line for [1] = 0 M hints at a possible rather high activity with W_0 ca. 1×10^{-5} M s^{-1} in the absence of **1**. However, the reaction rate of the metal-free reaction was determined to be 3 orders lower, being equal to 6×10^{-8} M s^{-1}. The reaction rate of chlorobenzene accumulation also follows the concentration of **1** (Figure 4), confirming that chlorobenzene by-product originates from the metal-catalyzed process rather than from spontaneous decomposition of *m*-CPBA.

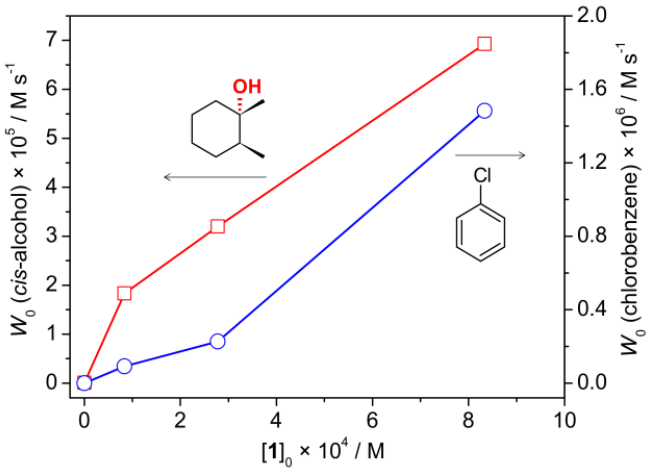

Figure 4. Dependences (experimental points) of the reaction rates of tertiary *cis*-alcohol (red squares) and chlorobenzene (blue circles) accumulations on concentration of **1** in the course of *cis*-1,2-DMCH oxidation with [*cis*-1,2-DMCH]$_0$ = 0.1 M, [*m*-CPBA]$_0$ = 2.7 × 10^{-2} M, [promoter]$_0$ = 5.5 × 10^{-3} M, [1]$_0$ = 2.8 × 10^{-4} M in CH_3CN (5 mL total volume) at 40 °C.

Table 1. Oxidation of *cis*-1,2-dimethylcyclohexane with *m*-CPBA, catalyzed by **1**, in the presence of promoters.[1]

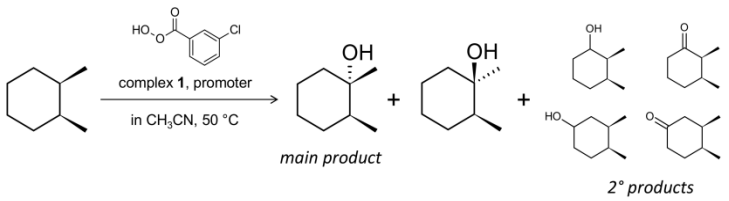

Entry	Promoter	[Cat]$_0$, mol%[2]	Yield, %[3]	Yield, %[4]	*cis*/*trans*[5]	TON[6]	3° : 2°[7]
1	HNO_3	0.08	17	61	82	198	38 : 1
2	HNO_3	0.8	11	40	82	13	38 : 1
3	HNO_3	0.3	14	50	90	48	38 : 1
4[8]	HNO_3	0.3	37	37	29	56	37 : 1
5	HOTf[9]	0.3	< 1	< 1	> 40	< 1	-
6	TFA[10]	0.3	7	26	16	25	24 : 1
7	HOAc[11]	0.3	6	24	11	25	19 : 1
8	PCA[12]	0.3	< 1	< 1	1	< 1	-
9	Et_3N	0.3	2	6	1	2.2	-
10	Py[13]	0.3	< 1	2	2	5.4	-
11[14]	HNO_3	0.3	14	51	78	59	40 : 1
12[15]	HNO_3	0.3	10	36	59	36	32 : 1

[1] General conditions are: [substrate]$_0$ = 0.1 M, [promoter]$_0$ = 5.5 × 10^{-3} M (5.5 mol% relative to substrate), [*m*-CPBA] = 2.7 × 10^{-2} M (0.27 equivalents relative to substrate), in acetonitrile, open air, at 40 °C, data shown are for 90 min reaction time; [2] relative to substrate; [3] yield (sum of 3° and 2° products) based on substrate; [4] yield (sum of 3° and 2° products) based on *m*-CPBA; [5] mols of tertiary *cis*-alcohol per mol of *trans*-alcohol; [6] turnover numbers, mols of products (sum of 3° and 2° products) per mol of catalyst; [7] normalized bond selectivity, (4 × mols of 3° products) / mol of 2° products; [8] [substrate]$_0$ = [*m*-CPBA]$_0$ = 0.05 M; [9] trifluoromethanesulfonic acid; [10] trifluoroacetic acid; [11] acetic acid; [12] pyrazinecarboxylic acid; [13] pyridine; [14] the complex $[Co^{III}Cd^{II}L_3Cl_2]\cdot 0.5H_2O$ [45] was used as a catalyst; [15] the complex $[CoL_3]\bullet$DMF [45] was used as a catalyst.

Since promoters may play a significant role in the peroxidative oxidation of alkanes and enhance yields and selectivities [2], we screened various promoting agents for the present system. Replacing nitric acid with a promoter of a higher Brønsted acidity [46,47], trifluoromethanesulfonic acid (HOTf), led to complete loss of activity showing negligible yields of products (Table 1, Entry 5). With weaker acids, such as acetic (HOAc) or trifluoroacetic (TFA) ones (Entries 7,6, respectively), the catalytic

process retains stereoselectivity, although the *cis*/*trans* ratio becomes much lower, corresponding to the retention of stereoconfiguration indexes (RC) of 85% and 89% for HOAc and TFA, respectively. Pyrazinecarboxylic acid (PCA) is a recognized promoter in the catalytic oxidation of C–H bonds with H_2O_2 due to its specific mechanism of action [48]. However, in the present case the **1**/PCA/*m*-CPBA system showed only trace yields of products, also demonstrating no stereoselectivity (Entry 8). Basic promoters, Et_3N and pyridine showed negligible activity (Entries 9,10, respectively). In the cases of Entries 5,8–10 the yields of products formed through the oxidation of methylenic sites of *cis*-1,2-DMCH were not sufficient for reliable determination of 3° : 2° bond selectivity. In all studied cases, no products of oxidation of primary carbon (methyl group) were detected, implying that the catalytic system is not able to oxidize them.

Hence, nitric acid has proven to be the most efficient promoter (Table 1). Within the respective tests (Entries 1–3), the conditions of Entry 3 were chosen as the optimal ones. Entry 1, while providing higher yields of products (61%), shows lower stereoselectivity with the *cis*/*trans* ratio of 82 (Table 1) what corresponds to 99.3% RC index. The test with elevated $[1]_0$ (Entry 3) shows a higher *cis*/*trans* ratio (Table 1) reaching the maximum RC of 99.5%, that reflects an almost complete stereospecificity of the catalytic process. We attempted to increase the yields of products based on the substrate by lowering the concentration of substrate to 0.05 M and using 1 equiv. of the oxidant (Table 1, Entry 4). Although the yield based on the substrate increases up to 37% comparing to 17% for Entry 1, the stereoselectivity drops down to *cis*/*trans* = 29, keeping nearly the same bond selectivity of 37 : 1 (Table 1).

The accumulation curves for HNO_3, TFA and HOAc promoters are given in Figure 5a. As can be seen, while the concentration of *cis*-tertiary alcohols continuously grows for the cases of TFA and HOAc, the HNO_3 one shows a maximum at 40 min with the yield of the tertiary *cis*-alcohol of 52% (59% for sum of 3° and 2° products), which is considerably higher than 45% exhibited at 90 min (50% for sum of all products, Entry 3). The yield decay in the 40–90 min interval could be related to overoxidation processes with the appearance of reaction by-products, particularly 2,7-octanedione (Figure S6). It is presumably formed through the attack at a second tertiary C–H bond of the *cis*-alcohol and subsequent cyclohexane ring cleavage.

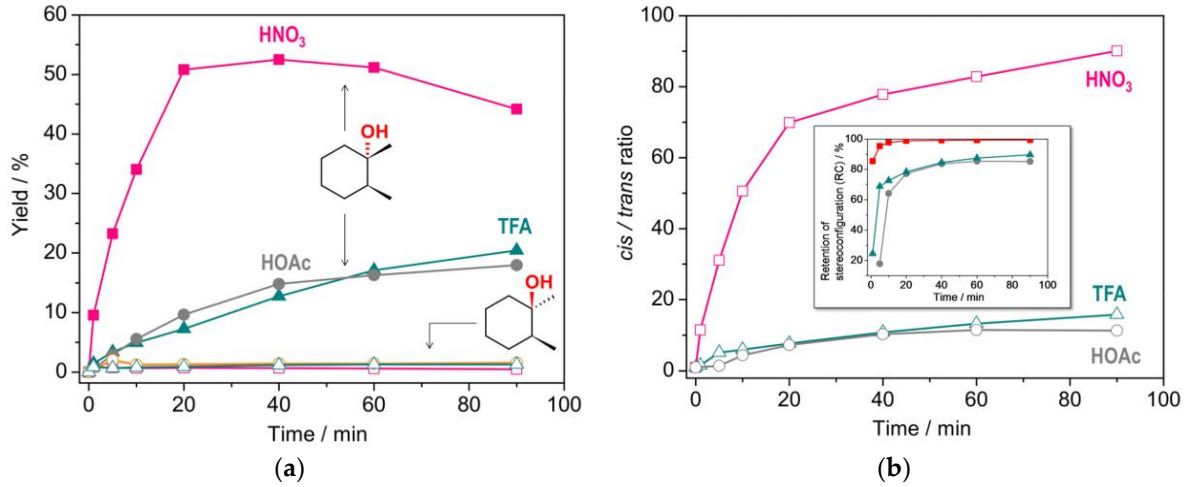

Figure 5. (**a**) Accumulations of tertiary *cis*- and *trans*-alcohols in *cis*-1,2-DMCH oxidation. Conditions are as those for Entries 3,6,7, Table 1; (**b**) The same entries, plotted as dependences of *cis*/*trans* ratios and retention of stereoconfiguration index (RC, inset).

Oxidation of dimethylcyclohexane isomers was performed to evaluate the selectivity features of the **1**/HNO_3/*m*-CPBA system towards a family of substrates with close structures. Previously for an acid-free system oxidizing with *m*-CPBA we have shown that *cis*-1,4-DMCH affords almost twice lower yields than its 1,2-isomer [26]. Herein the yields of products in the course of oxidations of 1,4-isomers (Table 2, Entries 2,4) are higher than those of 1,2-isomers (Table 2, Entries 1,3).

The 1,4-substrates show lower stereoselectivities than their 1,2-isomers (Table 2). The principal difference between *cis*- and *trans*-substrates lies in the 3° : 2° selectivity, which is considerably lower for *trans*-dimethylcyclohexanes. Oxidation of adamantane revealed the high normalized 3° : 2° bond selectivity of 39 : 1 and the highest yield of 71% among the substrates studied (Table 2, Entry 5).

The UV/Vis spectrum of the solution of **1** (1.4×10^{-4} M) in acetonitrile shows a number of absorption bands, with the most pronounced one at 370 nm and a very weak broad band at 680 nm (Figure 6a, inset, and Figure S7). The spectrum of **1** does not change with time suggesting the complex stability in CH_3CN solution. The band at 370 nm can be assigned to intraligand $\pi \rightarrow \pi^*$ transitions, while the second one (680 nm) could be due to phenolato-to-cobalt transfer [49,50]. The addition of HNO_3 (final concentration 5.5×10^{-3} M) leads to strong increase of the 370 nm absorption and appearance of a new band at 553 nm. The spectrum exhibits changes within ca. 5 min after addition of HNO_3, showing isosbestic points at 389, 420 and 669 nm (Figure 6a and Figure S8). Further addition of substrate, *cis*-1,2-DMCH, and then *m*-CPBA, in a minimum amount of acetonitrile to reach the final concentration of 1.3×10^{-3} M, leads to an overall intensity decrease with time, as evidenced by monitoring of the 370 nm band, finally showing broad absorption with no clear bands in the visible region (Figure 6b). These results may suggest that complex **1** undergoes transformation upon addition of the promoting agent. However, no expulsion of the ligand can be assumed as free HL has strong absorption at much higher energy at wavelength of 320 nm (Figure S9).

Table 2. Oxidation of dimethylcyclohexane isomers and adamantane. [1]

Entry	Substrate	Yield based on *m*-CPBA, %[2]	*cis*/*trans*	3° : 2°
1	*cis*-1,2-DMCH	50	90	38 : 1
2	*cis*-1,4-DMCH	64	42	22 : 1
3	*trans*-1,2-DMCH	46	62[3]	13 : 1
4	*trans*-1,4-DMCH	49	37[3]	12 : 1
5	Adamantane	71[4]	–	39 : 1

[1] Reaction conditions and other parameters are as those stated in the Table 1 footnote, unless stated otherwise. Entry 1 is Entry 3 in Table 1; [2] yield (sum of 3° and 2° products) based on *m*-CPBA; [3] *trans*/*cis* ratio, as the *trans*-substrates produce *trans*-alcohols as the main products; [4] sum of 3° and 2° products, where 3° products constitute 1-adamantanol and 1,3-adamantanediol (*ca.* 5%).

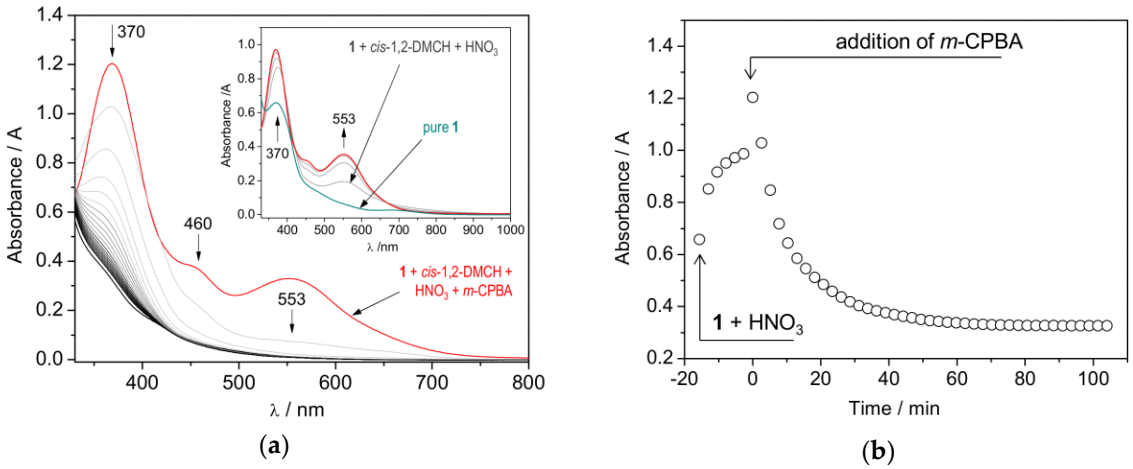

Figure 6. (**a**), inset: UV/Vis spectra of **1** in acetonitrile (1.4×10^{-4} M) (blue line). Grey lines are spectra measured after addition of *cis*-1,2-DMCH (0.05 M) and HNO_3 (5.5×10^{-3} M) to the above solution of **1**. Red line corresponds to the spectrum measured after 16 min. (**a**), main figure: *m*-CPBA (1.3×10^{-3} M) was added to the above solution of **1**, *cis*-1,2-DMCH and HNO_3 in acetonitrile. Red line corresponds to the spectrum measured immediately after addition of *m*-CPBA, black line shows the spectrum after 100 min. All the above-mentioned concentrations refer to those in the final solution; (**b**): Changes in the absorbance at 370 nm, plotted as a function of time.

Retention of stereoconfiguration at the sp^3 carbon atom in the course of C–H oxidation is a significant indicator of the absence of long-lived carbon-centered radicals as reaction intermediates [2]. Pronounced stereospecificity in the case of **1**/HNO_3/*m*-CPBA systems (Entries 1–4, Table 1) may account for the concerted or radical rebound mechanism, which does not involve long-lived radicals. In contrast, for the **1**/TFA/*m*-CPBA and **1**/HOAc/*m*-CPBA systems a much lower stereospecificity is observed, where inversion of the stereoconfiguration of the alkane substrate most probably comes from the presence of free carbon-centered radicals [2,35]. From these observations, as well as from the previous data [26,45,51], we assume that the overall reaction proceeds by two pathways, one possessing absolute stereospecificity and the other with epimerization of the stereoconfiguration of the substrate. Since dioxygen is a suitable radical trap for long-lived alkyl centered radicals [37–41] we performed oxidations using HNO_3 and HOAc promoters under the atmosphere of labelled dioxygen, $^{18}O_2$. Reaction of $^{18}O_2$ with C• radical produces labelled alcohol as a final product, which formation can be tracked by mass-spectroscopic methods [37–41]:

$$R_3C\bullet + {}^{18}O_2 \rightarrow R_3C\text{-}{}^{18}O{}^{18}O\bullet \rightarrow R_3C\text{-}{}^{18}OH$$

We expected that the system showing lower retention of stereoconfiguration would produce more ^{18}O-labelled products, as it happens for iron-catalyzed oxidations with H_2O_2 [36,52]. *cis*-1,2-DMCH oxidation in the presence of HNO_3 promoter, under $^{18}O_2$, revealed pure tertiary alcohols free of ^{18}O isotope (Figure S10). In contrast, the system involving acetic acid promoter showed large incorporation of ^{18}O, up to 68% in the *trans*-alcohol and up to 14% in the *cis*-one (Figure 7a). The accumulations of ^{18}O-labelled tertiary alcohols demonstrate similar initial reaction rates (Figure 7b), with the *cis*/*trans* ratios of the ^{18}O-alcohols ranging from 0.9 to 1.6 (Figure 7b, inset). Such values are typical for a free-radical oxidation of alkanes, for example, with hydroxyl radicals being attacking species [40,53].

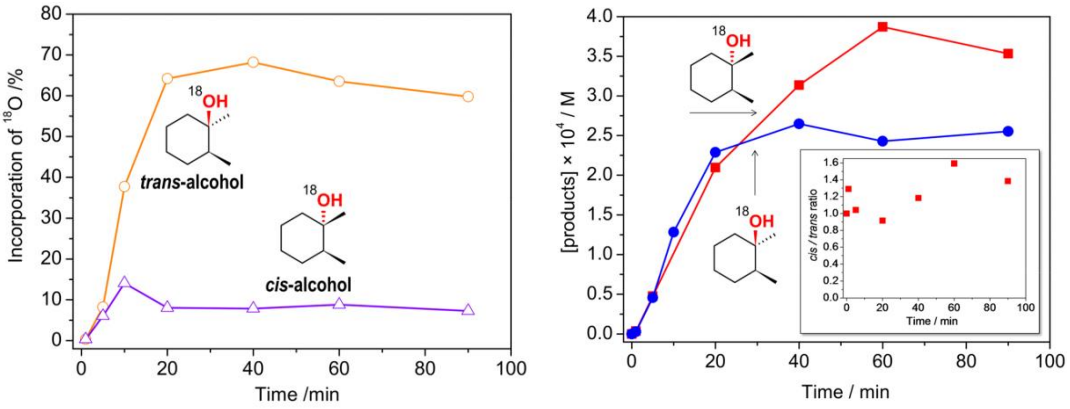

Figure 7. (**a**): ^{18}O incorporation into the tertiary alcohols in the process of *cis*-1,2-DMCH oxidation using HOAc promoter (Entry 7, Table 1) under atmosphere of $^{18}O_2$; (**b**): Accumulations of ^{18}O-labelled tertiary alcohols in the same reaction. Inset shows *cis*/*trans* ratio for ^{18}O-alcohols.

No difference between chromatograms recorded before and after the treatment of the sample with the solid PPh_3 was observed, suggesting that alkyl hydroperoxides are either not formed or are not stable under the experiment conditions [54]. Careful investigation of the chromatograms revealed that the ketones, formed through the oxidation of secondary sites of *cis*-1,2-DMCH, as well as the 2,7-octanedione by-product, contain large amounts of $^{18}O_2$ (*ca*. 70%) in the case of HOAc promoter. In contrary, the respective products formed in the HNO_3-promoted system contained ^{16}O isotope only. Ketones are known to rapidly exchange their oxygen with water via a metal-free mechanism [39,55]; hence the $^{18}O/^{16}O$ composition of ketones reflects the respective $H_2{}^{18}O/H_2{}^{16}O$ ratio in the reaction mixture. This means that the **1**/HOAc/*m*-CPBA/$^{18}O_2$ system leads to the formation of $H_2{}^{18}O$, probably coming from the spontaneous decomposition of ^{18}O-labelled peroxide species (Scheme 2).

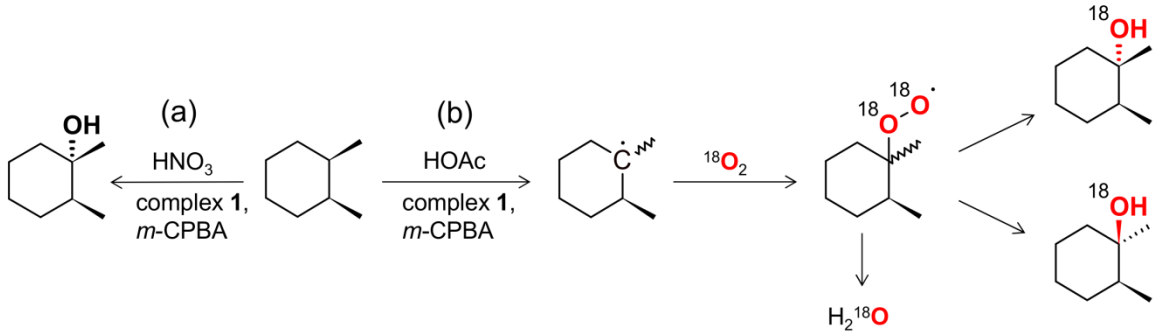

Scheme 2. Two dominant reaction pathways proposed for the (**a**) **1**/HNO_3/*m*-CPBA and (**b**) **1**/HOAc/*m*-CPBA catalytic systems. Pathway (**b**), in contrast to (**a**), proceeds via formation of a long-lived free carbon radical.

3. Materials and Methods

3.1. Reagents and General Procedures

2-Hydroxy-3-methoxy-benzaldehyde (*o*-vanillin) is commercially available (Sigma-Aldrich) and was used as received. All other chemicals were purchased from local suppliers and used without further purification. Elemental analyses (C, H, N) were performed with a PerkinElmer 2400 series analyzer. Infrared spectra (KBr pellets, 4000–400 cm^{-1}) were recorded using a BX-FT IR Perkin Elmer instrument. UV/Vis spectroscopy measurements were carried out on a Perkin-Elmer Lambda 35 spectrometer. ESI–MS(±) spectra were run on a LCQ Fleet mass spectrometer equipped with an electrospray (ESI) ion source (Thermo Scientific), using *ca.* 10^{-5} M solution of **1** in acetonitrile. The ^{1}H NMR spectra of complex **1** and HL in DMSO-*d*6 were measured at room temperature with a Mercury 400 Varian spectrometer at 400 MHz. The chemical shifts (δ) values are given in ppm downfield from internal Me_4Si. The ^{13}C NMR spectrum was recorded on Bruker Avance II+ 300 MHz (UltraShield™ Plus Magnet) spectrometer at ambient temperature.

The pro-ligand HL was prepared according to a reported procedure that was slightly modified [56]. In the synthesis of **1**, the reaction of condensation between *o*-vanillin and CH_3NH_2·HCl was used without isolation of the Schiff base.

3.2. Synthesis of [$CoZnL_3Cl_2$]·CH_3OH (1)

A mixture of *o*-vanillin (0.23 g, 1.5 mmol), CH_3NH_2·HCl (0.10 g, 1.5 mmol), dimethylaminoethanol (0.1 mL) and methanol (10 mL) in a 50 mL conic flask was stirred magnetically at 60 °C for half an hour. $CoCl_2$·$6H_2O$ (0.12 g, 0.5 mmol) dissolved in methanol (5 mL) was added to the yellow solution of the formed Schiff base, and the stirring continued for another 40 mins at the same temperature. After that, 0.03 g (0.5 mmol) of Zn powder was added to the flask and the mixture was stirred for an hour to achieve the total dissolution of the metal powder. Filtration and evaporation of the resultant brown solution at room temperature afforded dark-red crystals of complex **1** by the following day. The crystals were collected by filtration and washed with Pr^iOH (2 × 7 mL). Slow evaporation of the mother liquor produced more product. Yield: 50%. Anal. Calcd. for [$CoZnL_3Cl_2$]·CH_3OH (719.78): C 46.72, H 4.76, N 5.84%. Found: C 46.11, H 4.54, N 5.60%. ^{1}H NMR (400 MHz, DMSO-d_6, 21 °C): δ 7.95, 7.79, 7.46 (s, 3H, 3 × CH=N), 6.91–6.22 (m, 9H, 3 × C_6H_3), 3.61, 3.53 (s, 3H + 6H, 3 × OCH_3), 3.08 (s, 6H, 2 × NCH_3). ^{13}C NMR (75 MHz, DMSO-d_6, 21 °C, Figure S13): δ 168.19, 165.82, 165.33 (3 × CH=N), 157.76, 156.85, 155.03 (3 × C1), 153.09, 152.92, 152.82 (3 × C2), 126.62, 126.34, 126.27 (3 × C5), 121.99, 119.20, 118.82 (3×C6), 118.20, 117.70, 115.92 (3 × C4), 112.88, 112.49, 112.00 (3 × C3), 56.96, 56.89, 56.28 (3 × OCH_3), 47.36, 47.13, 46.58 (3 × NCH_3). FT–IR (KBr, ν, cm^{-1}): 3510*m*, 3444*m*, 3058*w*, 2938*m*, 2836*w*, 1630*s*, 1600*s*, 1568*w*, 1478*s*, 1462*s*, 1438*s*, 1402*w*, 1316*m*, 1300*s*, 1278*m*, 1254*vs*, 1230*s*, 1196*w*, 1080*m*, 1018*m*, 972*m*, 858*m*, 792*w*, 734*s*, 668*m*, 634*m*. FT–IR (KBr, ν, cm^{-1}): 3510*m*, 3444*m*, 3058*w*, 2938*m*, 2836*w*, 1630*s*, 1600*s*,

1568*w*, 1478*s*, 1462*s*, 1438*s*, 1402*w*, 1316*m*, 1300*s*, 1278*m*, 1254*vs*, 1230*s*, 1196*w*, 1080*m*, 1018*m*, 972*m*, 858*m*, 792*w*, 734*s*, 668*m*, 634*m*.

3.3. Single-crystal X-ray diffraction

Crystallographic data for the structure of **1** were collected at 100(2) K on an Oxford Diffraction Xcalibur diffractometer fitted with Mo Kα radiation. Following analytical absorption corrections and solution by direct methods, the structure was refined against F^2 with full-matrix least-squares using the program SHELXL-2017 [57]. The Co and Zn atoms were distinguished on the basis of refinement and coordination geometries. The solvent OH, H atom was refined with geometries restrained to ideal values. All remaining hydrogen atoms were added at calculated positions and refined by use of a riding model with isotropic displacement parameters based on those of the parent atom. Anisotropic displacement parameters were employed for the non-hydrogen atoms. The crystal data and structure refinement data are summarized in Table S2. CCDC 1833980 contains the supplementary crystallographic data for this paper.

3.4. Catalytic oxidation of alkanes

The reactions were typically carried out in air in thermostated cylindrical vials with vigorous stirring. Firstly, 0.9–2.1 mg of solid catalyst **1** was weighed into the reaction flask, then 3.4 or 3.5 mL of CH_3CN, 0.5 mL of CH_3NO_2 stock solution (internal standard; 1 mL of CH_3NO_2 mixed with 9 mL of CH_3CN), 2.1–50 μL of promoting agent (HNO_3, HOAc and TFA were used in a form of stock solutions in acetonitrile) and 70 μL of *cis*-1,2-dimethylcyclohexane were added. In the case of solid adamantane (68 mg), it was placed into the vial prior the addition of acetonitrile solution. Solid *m*-chloroperbenzoic acid (*m*-CPBA) oxidant was dissolved in acetonitrile (typically 30 mg in 1 mL of CH_3CN) and added dropwise within 10 seconds to a warm (40 °C) solution of other components under vigorous stirring. (CAUTION. The combination of *m*-CPBA with organic compounds at elevated temperatures may be explosive!). The total volume of the reaction solution was 5 mL. Samples were quenched at room temperature with excess of solid PPh_3 according to developed methods [54] and directly analyzed by GC and GC-MS techniques. Retention of stereoconfiguration (RC) index was calculated considering that the commercial substrate, *cis*-1,2-dimethylcyclohexane, contained 0.86% of *trans*-isomer.

3.5. Catalytic Reactions under $^{18}O_2$ Atmosphere

The reactions were typically performed in a thermostated Schlenk tube under vigorous stirring. The reagents were introduced in the same order as for a normal catalytic reaction. After the addition of *m*-CPBA the Schlenk tube was closed with the septum, and the mixture was immediately frozen with liquid nitrogen; the gas atmosphere was pumped and filled with N_2 a few times to remove air. The frozen mixture was left to warm under vacuum (to degasify) until becoming liquid, and the above procedure was repeated. Finally, the Schlenk tube was filled with $^{18}O_2$ through the septum, and the reaction mixture was heated at 40 °C with a possibility of gas to escape to compensate the excessive pressure. The $^{16}O/^{18}O$ compositions of the tertiary alcohols were determined by the relative abundance of 128/130 m/z mass peaks.

3.6. Gas Chromatography

A Perkin-Elmer Clarus 600 gas chromatograph equipped with two non-polar capillary columns (SGE BPX5; 30 m × 0.22 mm × 25 μm), one having an EI-MS (electron impact) detector and the other one with a FID detector, was used for analyses of the reaction mixtures. The following GC sequence has been used: 50 °C (3 min), 50–120 °C (8 degrees per minute), 120–300 °C (35 degrees per minute), 300 °C (3.11 min), 20 min total run time; 200 °C injector temperature. For analysis of oxidation products of highly-boiling compounds, such as adamantane, different conditioning was employed: 50 °C (3 min), 50–150 °C (30 degrees per minute), 150–300 °C (14 degrees per minute), 300 °C (2.95 min), 20 min

total run time; 200 °C injector temperature. Helium was used as the carrier gas with a constant 1 mL per minute flow. All EI–MS spectra were recorded with 70 eV energy. The identification of peaks at chromatograms was made by comparison of respective EI mass-spectra with those from the NIST v.2.0f database (PerkinElmer TurboMass v.5.4.2.1617 software). The mass-spectra patterns of tertiary dimethylcyclohexanols (Figure S12) were not found in the NIST database, and identification of these products was made by comparing with the reported previously mass-spectra [26,58].

4. Conclusions

In this work we have synthesized the novel complex $[Co^{III}Zn^{II}L_3Cl_2]\cdot CH_3OH$ (**1**) starting from zerovalent zinc, cobalt(II) chloride and using the *in situ* formed Schiff base pro-ligand HL. Single crystal X-ray analysis showed a binuclear core with O-bridging between the two different metal centers. The NMR studies of **1** suggested that the complex keeps its integrity in solution, while the results of ESI-MS investigations do not exclude some alterations of the structure of **1** with formation of larger polynuclear species under the ESI-MS conditions. The catalytic features of **1** were studied in the mild hydroxylation of alkane C–H bonds with *m*-CPBA oxidant, in the presence of a wide range of co-catalysts (promoters). The influence of the nature of the promoting agents on the catalytic efficiency was studied, revealing nitric acid as the best one, which provides up to 61% yield and >99% retention of stereoconfiguration.

The stereospecific properties of the catalytic system **1**/HNO_3/*m*-CPBA were tested on various isomers of dimethylcyclohexane as model substrates. Based on the selectivity and $^{18}O_2$ isotopic labelling data it was proposed that the **1**/Promoter/*m*-CPBA systems operate via two general reaction pathways, a stereospecific and a non-stereospecific one, which were distinguished by different incorporations of ^{18}O from $^{18}O_2$ into the alcohol products. The acetic acid promoter was found to enhance the non-selective process with a high level of epimerization of stereoconfiguration of substrate, while at the same time showing a large incorporation of ^{18}O from $^{18}O_2$ that was explained by the involvement of a long-lived carbon radical. In contrast, the nitric acid promoter showed a high retention of stereoconfiguration and a complete absence of ^{18}O in the reaction products, conceivably involving a metal based oxidant.

Supplementary Materials: The following are available online at http://www.mdpi.com/2073-4344/9/3/209/s1: Figure S1: IR-spectra of $[CoZnL_3Cl_2]\bullet CH_3OH$ (**1**) and HL; Figure S2: 400 MHz 1H NMR spectra of $[CoZnL_3Cl_2]\bullet CH_3OH$ (**1**) and HL in DMSO-*d6* at 294 K in the ranges of 0–18 and 1–14 ppm, respectively; Figure S3: ESI-MS spectrum of a solution of **1** in acetonitrile; Figure S4: Fragment of the ESI-MS spectrum of **1** (Figure S3) showing the isotopic distribution for the peak at 1338 *m/z*. The inset shows calculated distribution for the proposed species; Figure S5: Fragment of the ESI-MS spectrum of **1** (Figure S3) in acetonitrile showing the isotopic distribution for the peak at 1125 *m/z*. The inset shows calculated distribution for the proposed species; Figure S6: Fragment of the chromatogram showing the main reaction products and by-products in the course of *cis*-1,2-dimethylcyclohexane oxidation with *m*-CPBA catalyzed by **1** in the presence of HNO_3 promoter (Table 1, Entry 3); Figure S7: Fragment of the UV/Vis spectrum of **1** in acetonitrile showing the band at 680 nm; Figure S8: Fragment of the UV/Vis spectra depicted in Figure 6, (**a**), inset (**1** + *cis*-1,2-DMCH + HNO_3), showing isosbestic points; Figure S9: UV/Vis spectrum of free HL in acetonitrile (10^{-4} M); Figure S10: Fragments of the chromatograms, showing the intensities of 130 *m/z* signals (corresponding to the molecular ion, M+, of the ^{18}O-labelled tertiary alcohols) for the **1**/HOAc/*m*-CPBA and **1**/HNO_3/*m*-CPBA tests (Figure 7, 90 min); Figure S11: EI-MS spectra of the partially ^{18}O-labelled tertiary *trans*- and *cis*- alcohols, formed in the course of *cis*-1,2-DMCH oxidation catalyzed by **1** in the presence of HOAc promoter (Figure 7, 40 min); Figure S12: EI-MS spectra of the tertiary alcohols formed as the reaction products in the **1**/HNO_3/*m*-CPBA system (Table 2); Figure S13: ^{13}C NMR spectrum of $[CoZnL_3Cl_2]\bullet CH_3OH$ (**1**) in DMSO-*d6*; Table S1: Selected bond lengths (A) and angles (°) for $[CoZnL_3Cl_2]\bullet CH_3OH$ (**1**); Table S2: Crystal data and structure refinement for $[CoZnL_3Cl_2]\bullet CH_3OH$ (**1**).

Author Contributions: Conceptualization, O.V.N. and D.S.N.; methodology, O.V.N., D.S.N. and O.Y.V.; investigation, O.V.N., D.S.N., K.V.K., E.A.B. and B.W.S.; writing—original draft preparation, O.V.N., D.S.N. and O.Y.V.; writing—review and editing, A.J.L.P.

Funding: This work was supported by the Foundation for Science and Technology (FCT), Portugal (projects PTDC/QEQ-QIN/3967/2014, PTDC/QUI-QIN/29778/2017 and UID/QUI/00100/2013).

Acknowledgments: The authors acknowledge the IST Node of the Portuguese Network of Mass-spectrometry for the ESI-MS measurements.

Conflicts of Interest: The authors declare no conflicts.

References

1. Gensch, T.; James, M.J.; Dalton, T.; Glorius, F. Increasing Catalyst Efficiency in C–H Activation Catalysis. *Angew. Chem. Int. Ed.* **2018**, *57*, 2296–2306. [CrossRef] [PubMed]
2. Nesterov, D.S.; Nesterova, O.V.; Pombeiro, A.J.L. Homo- and heterometallic polynuclear transition metal catalysts for alkane C-H bonds oxidative functionalization: Recent advances. *Coord. Chem. Rev.* **2018**, *355*, 199–222. [CrossRef]
3. Ping, L.; Chung, D.S.; Bouffard, J.; Lee, S.-G. Transition metal-catalyzed site- and regio-divergent C–H bond functionalization. *Chem. Soc. Rev.* **2017**, *46*, 4299–4328. [CrossRef] [PubMed]
4. Tzouras, N.V.; Stamatopoulos, I.K.; Papastavrou, A.T.; Liori, A.A.; Vougioukalakis, G.C. Sustainable metal catalysis in C–H activation. *Coord. Chem. Rev.* **2017**, *343*, 25–138. [CrossRef]
5. Hartwig, J.F.; Larsen, M.A. Undirected, Homogeneous C–H Bond Functionalization: Challenges and Opportunities. *ACS Central Sci.* **2016**, *2*, 281–292. [CrossRef] [PubMed]
6. Cernak, T.; Dykstra, K.D.; Tyagarajan, S.; Vachal, P.; Krska, S.W. The medicinal chemist's toolbox for late stage functionalization of drug-like molecules. *Chem. Soc. Rev.* **2016**, *45*, 546–576. [CrossRef] [PubMed]
7. Hartwig, J.F. Evolution of C–H Bond Functionalization from Methane to Methodology. *J. Am. Chem. Soc.* **2016**, *138*, 2–24. [CrossRef] [PubMed]
8. Shul'pin, G.B. New Trends in Oxidative Functionalization of Carbon–Hydrogen Bonds: A Review. *Catalysts* **2016**, *6*, 50. [CrossRef]
9. Chu, J.C.K.; Rovis, T. Complementary Strategies for Directed C(sp^3)-H Functionalization: A Comparison of Transition-Metal-Catalyzed Activation, Hydrogen Atom Transfer, and Carbene/Nitrene Transfer. *Angew. Chem. Int. Ed.* **2018**, *57*, 62–101. [CrossRef] [PubMed]
10. He, J.; Wasa, M.; Chan, K.S.L.; Shao, O.; Yu, J.Q. Palladium-Catalyzed Transformations of Alkyl C–H Bonds. *Chem. Rev.* **2017**, *117*, 8754–8786. [CrossRef] [PubMed]
11. O'Reilly, E.; Kohler, V.; Flitsch, S.L.; Turner, N.J. Cytochromes P450 as useful biocatalysts: addressing the limitations. *Chem. Commun.* **2011**, *47*, 2490–2501. [CrossRef] [PubMed]
12. De Montellano, P.R.O. Hydrocarbon Hydroxylation by Cytochrome P450 Enzymes. *Chem. Rev.* **2010**, *110*, 932–948. [CrossRef] [PubMed]
13. Bryliakov, K.P.; Talsi, E.P. Active sites and mechanisms of bioinspired oxidation with H_2O_2, catalyzed by non-heme Fe and related Mn complexes. *Coord. Chem. Rev.* **2014**, *276*, 73–96. [CrossRef]
14. Wang, V.C.C.; Maji, S.; Chen, P.R.Y.; Lee, H.K.; Yu, S.S.F.; Chan, S.I. Alkane Oxidation: Methane Monooxygenases, Related Enzymes, and Their Biomimetics. *Chem. Rev.* **2017**, *117*, 8574–8621. [CrossRef] [PubMed]
15. Ray, K.; Pfaff, F.F.; Wang, B.; Nam, W. Status of Reactive Non-Heme Metal-Oxygen Intermediates in Chemical and Enzymatic Reactions. *J. Am. Chem. Soc.* **2014**, *136*, 13942–13958. [CrossRef] [PubMed]
16. Olivo, G.; Cusso, O.; Borrell, M.; Costas, M. Oxidation of alkane and alkene moieties with biologically inspired nonheme iron catalysts and hydrogen peroxide: from free radicals to stereoselective transformations. *J. Biol. Inorg. Chem.* **2017**, *22*, 425–452. [CrossRef] [PubMed]
17. Nam, W.; Lee, Y.M.; Fukuzumi, S. Tuning Reactivity and Mechanism in Oxidation Reactions by Mononuclear Nonheme Iron(IV)-Oxo Complexes. *Acc. Chem. Res.* **2014**, *47*, 1146–1154. [CrossRef] [PubMed]
18. Wang, S.; Chen, S.Y.; Yu, X.Q. C-H functionalization by high-valent Cp*Co(III) catalysis. *Chem. Commun.* **2017**, *53*, 3165–3180. [CrossRef] [PubMed]
19. Tan, P.W.; Mak, A.M.; Sullivan, M.B.; Dixon, D.J.; Seayad, J. Thioamide-Directed Cobalt(III)-Catalyzed Selective Amidation of C(sp^3)-H Bonds. *Angew. Chem. Int. Ed.* **2017**, *56*, 16550–16554. [CrossRef] [PubMed]
20. Kommagalla, Y.; Chatani, N. Cobalt(II)-catalyzed C-H functionalization using an N,N'-bidentate directing group. *Coord. Chem. Rev.* **2017**, *350*, 117–135. [CrossRef]
21. Michigami, K.; Mita, T.; Sato, Y. Cobalt-Catalyzed Allylic C(sp^3)-H Carboxylation with CO_2. *J. Am. Chem. Soc.* **2017**, *139*, 6094–6097. [CrossRef] [PubMed]
22. Barsu, N.; Bolli, S.K.; Sundararaju, B. Cobalt catalyzed carbonylation of unactivated C(sp^3)-H bonds. *Chem. Sci.* **2017**, *8*, 2431–2435. [CrossRef] [PubMed]

23. Shul'pin, G.B.; Loginov, D.A.; Shul'pina, L.S.; Ikonnikov, N.S.; Idrisov, V.O.; Vinogradov, M.M.; Osipov, S.N.; Nelyubina, Y.V.; Tyubaeva, P.M. Stereoselective Alkane Oxidation with *meta*-Chloroperoxybenzoic Acid (MCPBA) Catalyzed by Organometallic Cobalt Complexes. *Molecules* **2016**, *21*, 1593. [CrossRef] [PubMed]
24. Li, Q.; Hu, W.P.; Hu, R.J.; Lu, H.J.; Li, G.G. Cobalt-Catalyzed Cross-Dehydrogenative Coupling Reaction between Unactivated C(sp^2)-H and C(sp^3)-H Bonds. *Org. Lett.* **2017**, *19*, 4676–4679. [CrossRef] [PubMed]
25. Nesterova, O.V.; Nesterov, D.S. Polynuclear Cobalt Complexes as Catalysts for Light-Driven Water Oxidation: A Review of Recent Advances. *Catalysts* **2018**, *8*, 602. [CrossRef]
26. Nesterova, O.V.; Kopylovich, M.N.; Nesterov, D.S. Stereoselective oxidation of alkanes with *m*-CPBA as an oxidant and cobalt complex with isoindole-based ligands as catalysts. *RSC Adv.* **2016**, *6*, 93756–93767. [CrossRef]
27. Nesterov, D.S.; Nesterova, O.V.; Kokozay, V.N.; Pombeiro, A.J.L. Polynuclear Heterometallic Complexes from Metal Powders: The "Direct Synthesis" Approach. *Eur. J. Inorg. Chem.* **2014**, 4496–4517. [CrossRef]
28. Novikov, A.S.; Kuznetsov, M.L.; Rocha, B.G.M.; Pombeiro, A.J.L.; Shul'pin, G.B. Oxidation of olefins with H_2O_2 catalysed by salts of group III metals (Ga, In, Sc, Y and La): epoxidation versus hydroperoxidation. *Catal. Sci. Technol.* **2016**, *6*, 1343–1356. [CrossRef]
29. Kuznetsov, M.L.; Rocha, B.G.M.; Pombeiro, A.J.L.; Shul'pin, G.B. Oxidation of Olefins with Hydrogen Peroxide Catalyzed by Bismuth Salts: A Mechanistic Study. *ACS Catal.* **2015**, *5*, 3823–3835. [CrossRef]
30. Rocha, B.G.M.; Kuznetsov, M.L.; Kozlov, Y.N.; Pombeiro, A.J.L.; Shul'pin, G.B. Simple soluble Bi(III) salts as efficient catalysts for the oxidation of alkanes with H_2O_2. *Catal. Sci. Technol.* **2015**, *5*, 2174–2187. [CrossRef]
31. Kuznetsov, M.L.; Teixeira, F.A.; Bokach, N.A.; Pombeiro, A.J.L.; Shul'pin, G.B. Radical decomposition of hydrogen peroxide catalyzed by aqua complexes $[M(H_2O)_n]^{2+}$ (M = Be, Zn, Cd). *J. Catal.* **2014**, *313*, 135–148. [CrossRef]
32. Novikov, A.S.; Kuznetsov, M.L.; Pombeiro, A.J.L.; Bokach, N.A.; Shul'pin, G.B. Generation of HO• Radical from Hydrogen Peroxide Catalyzed by Aqua Complexes of the Group III Metals $[M(H_2O)_n]^{3+}$ (M = Ga, In, Sc, Y, or La): A Theoretical Study. *ACS Catal.* **2013**, *3*, 1195–1208. [CrossRef]
33. Gamba, I.; Codola, Z.; Lloret-Fillol, J.; Costas, M. Making and breaking of the O-O bond at iron complexes. *Coord. Chem. Rev.* **2017**, *334*, 2–24. [CrossRef]
34. Fukuzumi, S.; Kojima, T.; Lee, Y.M.; Nam, W. High-valent metal-oxo complexes generated in catalytic oxidation reactions using water as an oxygen source. *Coord. Chem. Rev.* **2017**, *333*, 44–56. [CrossRef]
35. Olivo, G.; Lanzalunga, O.; Di Stefano, S. Non-Heme Imine-Based Iron Complexes as Catalysts for Oxidative Processes. *Adv. Synth. Catal.* **2016**, *358*, 843–863. [CrossRef]
36. Chen, K.; Que, L. Stereospecific alkane hydroxylation by non-heme iron catalysts: Mechanistic evidence for an Fe-V = O active species. *J. Am. Chem. Soc.* **2001**, *123*, 6327–6337. [CrossRef] [PubMed]
37. Gryca, I.; Czerwinska, K.; Machura, B.; Chrobok, A.; Shul'pina, L.S.; Kuznetsov, M.L.; Nesterov, D.S.; Kozlov, Y.N.; Pombeiro, A.J.L.; Varyan, I.A.; et al. High Catalytic Activity of Vanadium Complexes in Alkane Oxidations with Hydrogen Peroxide: An Effect of 8-Hydroxyquinoline Derivatives as Noninnocent Ligands. *Inorg. Chem.* **2018**, *57*, 1824–1839. [CrossRef] [PubMed]
38. Shul'pin, G.B.; Nesterov, D.S.; Shul'pina, L.S.; Pombeiro, A.J.L. A hydroperoxo-rebound mechanism of alkane oxidation with hydrogen peroxide catalyzed by binuclear manganese(IV) complex in the presence of an acid with involvement of atmospheric dioxygen. *Inorg. Chim. Acta.* **2017**, *455*, 666–676. [CrossRef]
39. Bilyachenko, A.N.; Levitsky, M.M.; Yalymov, A.I.; Korlyukov, A.A.; Vologzhanina, A.V.; Kozlov, Y.N.; Shul'pina, L.S.; Nesterov, D.S.; Pombeiro, A.J.L.; Lamaty, F.; et al. A heterometallic (Fe_6Na_8) cage-like silsesquioxane: synthesis, structure, spin glass behavior and high catalytic activity. *RSC Adv.* **2016**, *6*, 48165–48180. [CrossRef]
40. Vinogradov, M.M.; Kozlov, Y.N.; Bilyachenko, A.N.; Nesterov, D.S.; Shul'pina, L.S.; Zubavichus, Y.V.; Pombeiro, A.J.L.; Levitsky, M.M.; Yalymov, A.I.; Shul'pin, G.B. Alkane oxidation with peroxides catalyzed by cage-like copper(II) silsesquioxanes. *New J. Chem.* **2015**, *39*, 187–199. [CrossRef]
41. Vinogradov, M.M.; Kozlov, Y.N.; Nesterov, D.S.; Shul'pina, L.S.; Pombeiro, A.J.L.; Shul'pin, G.B. Oxidation of hydrocarbons with H_2O_2/O_2 catalyzed by osmium complexes containing *p*-cymene ligands in acetonitrile. *Catal. Sci. Technol.* **2014**, *4*, 3214–3226. [CrossRef]
42. Vikse, K.L.; Ahmadi, Z.; McIndoe, J.S. The application of electrospray ionization mass spectrometry to homogeneous catalysis. *Coord. Chem. Rev.* **2014**, *279*, 96–114. [CrossRef]

43. Serrano-Plana, J.; Oloo, W.N.; Acosta-Rueda, L.; Meier, K.K.; Verdejo, B.; Garcia-Espana, E.; Basallote, M.G.; Munck, E.; Que, L.; Company, A.; et al. Trapping a Highly Reactive Nonheme Iron Intermediate That Oxygenates Strong C-H Bonds with Stereoretention. *J. Am. Chem. Soc.* **2015**, *137*, 15833–15842. [CrossRef] [PubMed]
44. Font, D.; Canta, M.; Milan, M.; Cusso, O.; Ribas, X.; Gebbink, R.J.M.K.; Costas, M. Readily Accessible Bulky Iron Catalysts exhibiting Site Selectivity in the Oxidation of Steroidal Substrates. *Angew. Chem. Int. Ed.* **2016**, *55*, 5776–5779. [CrossRef] [PubMed]
45. Nesterova, O.V.; Kasyanova, K.V.; Makhankova, V.G.; Kokozay, V.N.; Vassilyeva, O.Y.; Skelton, B.W.; Nesterov, D.S.; Pombeiro, A.J.L. Stereospecific sp^3 C-H oxidation with *m*-CPBA: A Co^{III} Schiff base complex as pre-catalyst vs. its $Co^{III}Cd^{II}$ heterometallic derivative. *Appl. Catal. A.* **2018**, *560*, 171–184. [CrossRef]
46. Raamat, E.; Kaupmees, K.; Ovsjannikov, G.; Trummal, A.; Kuett, A.; Saame, J.; Koppel, I.; Kaljurand, I.; Lipping, L.; Rodima, T.; et al. Acidities of strong neutral Bronsted acids in different media. *J. Phys. Org. Chem.* **2013**, *26*, 162–170. [CrossRef]
47. Muckerman, J.T.; Skone, J.H.; Ning, M.; Wasada-Tsutsui, Y. Toward the accurate calculation of pK(a) values in water and acetonitrile. *Bioenerg.* **2013**, *1827*, 882–891. [CrossRef] [PubMed]
48. Kirillov, A.M.; Shul'pin, G.B. Pyrazinecarboxylic acid and analogs: Highly efficient co-catalysts in the metal-complex-catalyzed oxidation of organic compounds. *Coord. Chem. Rev.* **2013**, *257*, 732–754. [CrossRef]
49. Allard, M.M.; Xavier, F.R.; Heeg, M.J.; Schlegel, H.B.; Verani, C.N. Sequential Phenolate Oxidations in Octahedral Cobalt(III) Complexes with N_2O_3 Ligands. *Eur. J. Inorg. Chem.* **2012**, 4622–4631. [CrossRef]
50. Nesterov, D.S.; Nesterova, O.V.; Guedes da Silva, M.F.C.; Pombeiro, A.J.L. Catalytic behaviour of a novel Fe(III) Schiff base complex in the mild oxidation of cyclohexane. *Catal. Sci. Technol.* **2015**, *5*, 1801–1812. [CrossRef]
51. Nesterov, D.S.; Nesterova, O.V.; Kopylovich, M.N.; Pombeiro, A.J.L. Pronounced retention of stereoconfiguration upon sp^3 C-H bonds hydroxylation of dimethylcyclohexanes and decahydronaphthalenes with *m*-CPBA oxidant and a Co-phthalocyanine catalyst. *Mol. Catal.* **2018**, *459*, 8–15. [CrossRef]
52. Ghosh, M.; Pattanayak, S.; Dhar, B.B.; Singh, K.K.; Panda, C.; Sen Gupta, S. Selective C-H Bond Oxidation Catalyzed by the Fe-bTAML Complex: Mechanistic Implications. *Inorg. Chem.* **2017**, *56*, 10852–10860. [CrossRef] [PubMed]
53. Nesterov, D.S.; Chygorin, E.N.; Kokozay, V.N.; Bon, V.V.; Boca, R.; Kozlov, Y.N.; Shul'pina, L.S.; Jezierska, J.; Ozarowski, A.; Pombeiro, A.J.L. Heterometallic $Co^{III}{}_4Fe^{III}{}_2$ Schiff Base Complex: Structure, Electron Paramagnetic Resonance, and Alkane Oxidation Catalytic Activity. *Inorg. Chem.* **2012**, *51*, 9110–9122. [CrossRef] [PubMed]
54. Shul'pin, G.B. Metal-catalyzed hydrocarbon oxygenations in solutions: The dramatic role of additives: A review. *J. Mol. Catal. A* **2002**, *189*, 39–66. [CrossRef]
55. Ottenbacher, R.V.; Samsonenko, D.G.; Talsi, E.P.; Bryliakov, K.P. Highly Enantioselective Bioinspired Epoxidation of Electron-Deficient Olefins with H_2O_2 on Aminopyridine Mn Catalysts. *ACS Catal.* **2014**, *4*, 1599–1606. [CrossRef]
56. Chatziefthimiou, S.D.; Lazarou, Y.G.; Hadjoudis, E.; Dziembowska, T.; Mavridis, I.M. Keto forms of salicylaldehyde Schiff bases: Structural and theoretical aspects. *J. Phys. Chem. B* **2006**, *110*, 23701–23709. [CrossRef] [PubMed]
57. Sheldrick, G.M. Crystal structure refinement with SHELXL. *Acta Cryst. C* **2015**, *71*, 3–8. [CrossRef] [PubMed]
58. Ottenbacher, R.V.; Talsi, E.P.; Bryliakov, K.P. Mechanism of Selective C-H Hydroxylation Mediated by Manganese Aminopyridine Enzyme Models. *ACS Catal.* **2015**, *5*, 39–44. [CrossRef]